Human Cancer Biology

Clinical Cancer Research

Costimulatory Protein 4IgB7H3 Drives the Malignant Phenotype of Glioblastoma by Mediating Immune Escape and Invasiveness

Dieter Lemke[1,3], Philipp-Niclas Pfenning[1], Felix Sahm[4], Ann-Catherine Klein[1], Tore Kempf[5], Uwe Warnken[5], Martina Schnölzer[5], Ruxandra Tudoran[2,3], Michael Weller[6], Michael Platten[2,3], and Wolfgang Wick[1,3]

Abstract

Purpose: Recent work points out a role of B7H3, a member of the B7-family of costimulatory proteins, in conveying immunosuppression and enforced invasiveness in a variety of tumor entities. Glioblastoma is armed with effective immunosuppressive properties resulting in an impaired recognition and ineffective attack of tumor cells by the immune system. In addition, extensive and diffuse invasion of tumor cells into the surrounding brain tissue limits the efficacy of local therapies. Here, 4IgB7H3 is assessed as diagnostic and therapeutic target for glioblastoma.

Experimental Design: To characterize B7H3 in glioblastoma, we conduct analyses not only in glioma cell lines and glioma-initiating cells but also in human glioma tissue specimens.

Results: B7H3 expression by tumor and endothelial cells correlates with the grade of malignancy in gliomas and with poor survival. Both soluble 4IgB7H3 in the supernatant of glioma cells and cell-bound 4IgB7H3 are functional and suppress natural killer cell–mediated tumor cell lysis. Gene silencing showed that membrane and soluble 4IgB7H3 convey a proinvasive phenotype in glioma cells and glioma-initiating cells *in vitro*. These proinvasive and immunosuppressive properties were confirmed *in vivo* by xenografted 4IgB7H3 gene silenced glioma-initiating cells, which invaded significantly less into the surrounding brain tissue in an orthotopic model and by subcutaneously injected LN-229 cells, which were more susceptible to natural killer cell–mediated cytotoxicity than unsilenced control cells.

Conclusions: Because of its immunosuppressive and proinvasive function, 4IgB7H3 may serve as a therapeutic target in the treatment of glioblastoma. *Clin Cancer Res; 18(1); 105–17. ©2011 AACR.*

Introduction

One of the key biologic features of glioblastoma is its ability to suppress the immune system resulting in an impaired recognition and attack of the tumor cells by the immune system. A number of factors have been identified within the last 2 decades that are held responsible for the immunosuppressive nature of glioblastomas (1–8). TGF-β turned out to induce apoptosis in T cells, to downregulate costimulatory proteins on cytotoxic T cells, natural killer (NK) cells, and glioma cells, as well as to upregulate immunosuppressive ligands on glioblastoma cells. In addition to the immunosuppressive properties, invasion of tumor cells into the surrounding brain tissue is another hallmark of human glioblastoma. This invasive behavior limits the feasibility of local treatment such as surgical tumor resection or involved-field radiotherapy. Glioblastoma cells usually invade as single cells migrating along white matter tracts implicating the involvement of integrin-mediated signalling pathways and the degradation of components of the extracellular matrix by matrix metalloproteinases (MMP). Recently, two isoforms of a novel member of the B7-family of costimulatory proteins, 2IgB7H3 and 4IgB7H3, have been identified (9, 10). The latter was more widely expressed in human maturating dendritic cells, T cells, and many human tumor cell lines including glioblastoma (11). 4IgB7H3 was initially supposed to convey T-cell activation and to induce IFN-γ production, but more recent evidence suggests that 4IgB7H3 expressed by different human malignancies suppresses NK cells and cytotoxic T cells. In this regard, NK-mediated lysis of neuroblastoma cell lines was

Authors' Affiliations: [1]Clinical Cooperation Unit Neurooncology and [2]Helmholtz Group for Experimental Neuroimmunology, German Cancer Research Center; Departments of [3]Neurooncology at the National Center for Tumor Diseases and [4]Neuropathology, University Hospital Heidelberg; [5]Protein Analysis Facility, German Cancer Research Center, Heidelberg, Germany; and [6]Department of Neurology, University Hospital Zurich, Zurich, Switzerland

Note: Supplementary data for this article are available at Clinical Cancer Research Online (http://clincancerres.aacrjournals.org/).

D. Lemke and P.-N. Pfenning contributed equally to this work.

Corresponding Author: Wolfgang Wick, Department of Neurooncology, University Hospital Heidelberg, Im Neuenheimer Feld 400, Heidelberg 69120, Germany. Phone: 49-6221-567075; Fax: 49-6221-567554; E-mail: wolfgang.wick@med.uni-heidelberg.de

doi: 10.1158/1078-0432.CCR-11-0880

Translational Relevance

Characteristic features of malignant gliomas are their immunosuppressive phenotype and infiltrative growth. Factors such as TGF-β are relevant in both processes. Here, we show that this is likewise the case for 4IgB7H3, a novel member of the B7-family of costimulatory proteins. We show B7H3 expression *in vivo* by glioblastoma and endothelial cells and show a correlation with the grade of malignancy and an association with worse clinical outcome. As opposed to other tumors and dendritic cells, 4lgB7H3 is functional in immune and invasion paradigms both in cell surface–bound and in a soluble form of 93 kDa. The soluble form was shown to lack the intracellular and the transmembrane domain and was identified in the supernatant of long-term and primary glioma cells. In summary, 4lgB7H3 is an interesting candidate for diagnostic and therapeutic purposes and pivotal for the glioma immune escape as well as gliomas cell invasiveness.

enhanced by 4IgB7H3-neutralizing antibodies (12). High expression of 4IgB7H3 is associated with a poor prognosis in different tumor entities (13–17). Apart from the expression on tumor cells, 4IgB7H3 is also specifically upregulated on tumor endothelia (18).

The ligand for B7H3 has not been identified yet. It was postulated that the ligand is expressed on activated T cells (9). Hashiguchi and colleagues (19) delineated triggering receptor expressed on myeloid cell-like transcript 2 (TLT-2) to be this receptor, but the interaction of B7H3 and TLT-2 resulted in T-cell activation, which could not explain its immunosuppressive action. Moreover, the physical interaction of B7H3 and TLT-2 was not confirmed (20). Finally, a soluble form of B7H3 was described to be expressed by human immune cells and by a variety of different tumor cells. This soluble form is cleaved by MMPs from the cell surface and is detected in increased levels in the serum of patients with non–small cell lung carcinoma compared with healthy controls and correlated with the tumor burden (21–23).

Factors such as TGF-β are relevant in both processes immunosuppression and invasiveness. Here, we show that this is likewise the case for 4lgB7H3. We show B7H3 expression *in vivo* by glioblastoma and endothelial cells. 4IgB7H3 was until date only detected in the glioblastoma cell lines U251, A172, and U87 (10). Furthermore, expression of B7H3 in human glioma correlates with the grade of malignancy of astrocytic tumors, ranging from World Health Organization (WHO) grade II to IV. Importantly, 4IgB7H3 is functional by suppressing NK cell–mediated tumor lysis *in vitro* and *in vivo*. Moreover, glioblastoma-derived soluble 4IgB7H3 suppresses NK cell lysis. So far, the soluble form in monocytes, dendritic cell, and activated T cells was published to be 16.5 kDa (22). This fragment differs from the 93-kDa fragment detected in the supernatant of glioma-initiating cell (GIC) cultures and glioma cell lines with commercial antibodies. This 93-kDa fragment was not cleaved by MMPs from the surface of glioblastoma cells but by serum endopeptidases. Finally, high B7H3 expression correlates with a lower invasion of CD8-positive cells in human glioblastoma tissue than low B7H3–expressing glioblastomas and 4IgB7H3 exerts a proinvasive effect on glioblastoma cells *in vitro* and more important *in vivo*.

Material and Methods

Cells and cell culture

LN-229 glioma cells were kindly provided by Dr. N. de Tribolet (Department of Neurosurgery, University Hospital, Lausanne, Switzerland). The cell line was maintained in Dulbecco's Modified Eagle's Medium containing 10% fetal calf serum and penicillin (100 IU/mL)/streptomycin (100 mg/mL; ref. 24). For the generation of GIC cultures, tumor samples were obtained from adult patients diagnosed with glioblastoma after informed consent. The tumor and the GIC culture methods were modified from the study of Svendsen and colleagues (25) as previously described (26). Glioma characteristic chromosomal abnormalities have been verified by array comparative genome hybridization (B. Radlwimmer, Department of Molecular genetics, German Cancer Research Center Heidelberg, Heidelberg, Germany). Lentiviral knockdown of 4IgB7H3 and control knockdown cells were produced with lentiviral short hairpin (sh) 4IgB7H3 and control particles from Santa Cruz Biotechnology (Cat. no.: sc-45444-V and sc-108080). The unselected 4IgB7H3 knockdown cells were named sh 4IgB7H3 pool cells. From these cells, a clonal knockdown was selected with a higher knockdown rate, which was termed sh 4IgB7H3 clone19. Human cerebral microvascular endothelial cells (HCMEC) and human brain vascular pericytes were purchased from Sciencell.

Lysates for immunoblots and cell culture supernatants were prepared as described previously (27, 28). Briefly, supernatants were generated for 72 hours after plating 3×10^6 cells in serum-free medium. Serum-free supernatants were concentrated with the Centriplus centrifugal filter device YM-3 (3,000-Da cutoff point; Millipore). Afterward, a Bradford assay was conducted to assure that equal amounts of supernatant-derived protein were used for the NK cell lysis assays or immunoblot analysis. To unravel the mechanisms of how 4IgB7H3 is cleaved by glioblastoma cells and how 4IgB7H3 is regulated, 1.25×10^6 LN-229 cells were seeded in serum-free medium and the following compounds and treatments were used:

1. To evaluate hypoxia, cells were incubated for 48 hours in serum-free medium under hypoxic conditions at 1% O_2 and compared with cells that were kept at 21% O_2.
2. To evaluate the influence of protein kinase C activation, cells were incubated with phorbol 12-myristate 13-acetate (PMA; Sigma-Aldrich) diluted in

dimethyl sulfoxide (DMSO) at a final concentration of 100 nmol/L for 48 hours (29).

3. The influence of TGF-β inhibition was tested with LY2157299, a TGF-β receptor kinase I inhibitor at 25 nmol/L (Axon Medchem BV; ref. 29) or the synthetic furin inhibitor, decanoyl-Arg-Val-Lys-Arg-chloromethylketone (dec-RVKR-cmk; Bachem), which was diluted in methanol. Cells were incubated at 15 μmol/L. New furin inhibitor was added every 12 hours (30).
4. To examine whether 4IgB7H3 is cleaved by MMP, the MMP inhibitor ilomastat (22) was used at concentrations of 5 to 10 μmol/L (Chemicon International). Respective DMSO controls were included.

Afterward, cells were collected to carry out quantitative real-time PCR (qRT-PCR), immunoblots of supernatants and lysates, and flow cytometric analysis. All compounds used were shown to be functional in other assays.

Immunoblot analysis

Cells were lysed in 50 mmol/L Tris-HCl (pH 8) containing 120 mmol/L NaCl, 5 mmol/L EDTA, 0.5% Nonidet P-40, 2 μg/mL aprotinin, 10 μg/mL leupeptin (Sigma-Aldrich), and 100 μg/mL phenylmethylsulfonylfluoride. Protein levels were analyzed by immunoblot using 30 μg of protein per lane with the respective antibodies in the concentrations recommended by the manufacturer (28). The antibodies used were goat polyclonal anti-human B7H3 (R&D) and rabbit anti-human anti-B7H3 antibody HPA 017139 (Atlas Antibodies). Protein bands were visualized using horseradish peroxidase–coupled secondary antibodies (Sigma-Aldrich). Equal protein loading was ascertained by Ponceau S staining as well as α-tubulin stainings with mouse anti-α-tubulin antibody (Sigma-Aldrich) and rabbit anti β-actin antibody (Cell Signalling).

Exosome isolation

Serum-free conditioned medium from human glioblastoma cells was collected after 48 hours. Microvesicles were purified by differential centrifugation steps (300 × *g* for 10 minutes; 2,000 × *g* for 20 minutes; and 10,000 × *g* for 30 minutes), pelleted by ultracentrifugation at 175,000 × g for 60 minutes, and washed in PBS. Exosomes were identified by immunoblotting using the exosomal marker protein CD9 (mouse anti-human CD9; 1:1,000; Chemicon Temecula).

Flow cytometry

For flow cytometry, cells were dissociated with accutase, washed and stained with goat polyclonal anti-human B7H3 1:100 (R&D) or respective isotype control. As secondary antibody, donkey Alexa 488 anti-goat antibody was used (Invitrogen), and fluorescence in a total of 10,000 events per condition was detected. Cells were analyzed with a BD-FACS Canto II flow cytometer (BD Biosciences), final data were processed with the help of FlowJo flow cytometry analysis software (Tree Star). Specific fluorescence intensity (SFI) was calculated by using the mean fluorescence signal of B7H3 divided by the mean fluorescence isotype signal.

qRT-PCR

Total RNA was extracted using a RNA purification system (Qiagen) and treated with RNase-free DNase I to remove genomic DNA (Roche). The cDNA was prepared from 5 mg of total RNA using Superscript RNase H-Reverse Transcriptase (Invitrogen) and random hexamers (Sigma-Aldrich). For qRT-PCR, gene expression was measured in an ABI Prism 7000 sequence detection system (Applied Biosystems) with SYBR Green Master Mix (Eurogentec) and primers at optimized concentrations (31). Primers (Sigma-Aldrich) were selected to span exon–exon junctions. The sequence for human *4IgB7H3* and the housekeeping gene glyceraldehyde-3-phosphate dehydrogenase (*GAPDH*) were as follows: 4IgB7H3 forward primer 5′-CATCACACCCCAGAGAAGCC-3′, reverse primer 5′-AGAGGGCCGTG CGGTTGGCA-3′, GAPDH primers have been described previously (32). Standard curves were generated for each gene and the amplification was 90% to 100% efficient. Relative quantification of gene expression was determined by comparison of threshold values. All results were normalized to GAPDH.

Mass spectrometry analysis

Probe preparation. The band corresponding to 4IgB7H3-immunostained areas on the immunoblot were excised from SDS-PAGE. Gel pieces were consecutively washed with water and 50% acetonitrile, reduced with 10 mmol/L diothreitol (DTT) at 56°C for 1 hour and alkylated with 55 mmol/L iodoacetamide (Sigma-Aldrich) at 25°C for 30 minutes in the dark. After alkylation, gel plugs were repeatedly washed with water and 50% acetonitrile, dehydrated with 100% acetonitrile, and air dried. The dried gel plugs were reswollen in 40 mmol/L ammonium bicarbonate containing 17 ng/μL sequencing grade–modified trypsin (Promega). Following enzymatic digestion overnight at 37°C, peptides were repeatedly extracted with 0.1% trifluoroacetic acid (TFA) and acetonitrile/0.1% TFA 50:50 (v/v). The combined solutions were dried in a speed-vac for 2 hours at 37°C. Peptides were redissolved in 5 μL 0.1% TFA by sonication for 10 minutes and applied for electrospray-tandem mass spectrometry (ESI-MS/MS) analysis.

Orbitrap mass spectrometric analysis. NanoLC-MS/MS analysis was conducted using the nanoACQUITY (Waters) coupled to a nanoESI-LTQ-Orbitrap mass spectrometer (Thermo Scientific) using a stepped linear acetonitrile/water gradient ranging from 5% to 90% within 45 minutes. For enhancing the number of detected peptides, a targeted proteomics approach was used for the identification of 4IgB7H3 (gi67188443, CD276 antigen isoform a, *Homo sapiens*). Only peptide masses obtained from an *in silico* trypsin digestion of 4IgB7H3 using an MS-Digest tool from the online ProteinProspector v5.7.2 software (UCSF, San Francisco, CA) were isolated and fragmented by Orbitrap. Processed data were searched against the NCBInr database using the Mascot algorithm version v2.2.0 (Matrix Science

Ltd.). The taxonomy *Homo sapiens* was selected for Mascot searches.

NK lysis assay

Peripheral blood lymphocytes (PBL) were isolated from whole blood samples of healthy donors by Ficoll-Hypaque density gradient centrifugation. NK cells were then isolated from PBLs by depletion of non–NK cells using an NK cell isolation kit (Miltenyi Biotec). Isolated $CD56^+/CD3^-$ NK cells were maintained in RPMI-1640 medium (PAA Laboratories) containing 10% FBS (Perbio) and 1,000 U/mL interleukin-2 (Immunotools) for 5 days at 37°C/5%CO_2.

NK cell cytotoxicity was assessed using ^{51}chromium (^{51}Cr)-release assay (3). Briefly, labeled glioma cells (5×10^3 per well) were seeded in triplicates into a U-shaped 96-well microtiter plate and incubated in triplicates with NK effector cells with effective target-to-effector ratios of 1:30, 1:10, and 1:3. Minimum and maximum ^{51}Cr release was determined by using target cells incubated in medium alone or 10% Triton X-100 (Applichem). After incubation at 37°C/5% CO_2 for 4 hours, supernatants were collected from each well and counted in a gamma counter (Packard). Specific NK lysis in percent was calculated as follows: (experimental ^{51}Cr release − minimum release)/(maximum release − minimum release) × 100.

Matrigel invasion assay

The invasive properties of glioma cells were assessed in Boyden chamber assays (BD Biosciences), where a porous membrane (8-μm pore size) coated with Matrigel matrix separates upper and lower wells. Glioma cells were harvested in enzyme-free cell dissociation buffer (Gibco Life Technologies), and a total of 4×10^4 cells in culture medium were added in triplicates to the upper chamber (33). NIH 3T3–conditioned medium (0.5 mL) was used as a chemoattractant in the bottom well. Cell invasion was evaluated by counting the number of cells that had migrated across the membrane in 5 independent fields and expressed as percentage of invasiveness relative to control.

Spheroid invasion assay

A total of 1×10^6 GICs were seeded in neural sphere cell medium (NSCM; Invitrogen) and kept in culture until spheroids had formed. Extracellular matrix gel was prepared as described previously (28). Glioma cell spheroids were seeded into the collagen gel solution in a 24-well plate in triplicates. After gelation, the gel was covered with medium and cultured at 37°C/5% CO_2. Microscopic images of the area covered by each spheroid were taken at 0, 24, 48, and 72 hours after implantation. For quantification, the mean area which was covered by invaded glioma cells at an indicated time point was measured in intervals of 24 hours and compared with the area at 0 hours.

Animal experiments

Animal work was approved by the governmental authorities (Regierungspräsidium Karlsruhe, Germany) and supervised by institutional animal protection officials in accordance with the NIH guidelines *Guide for the Care and Use of Laboratory Animals*.

Orthotopic brain tumor model

A total of 1×10^5 human T269 4IgB7H3 knockdown or T269 control cells were stereotactically implanted into the right striatum of five 6- to 12-week-old athymic mice (CD1 *nu/nu*; Charles River Laboratories), respectively. Ten weeks after implantation, animals were sacrificed, brains removed and cryosectioned. To access infiltration, immunostainings were conducted with rabbit anti-human nestin antibody (Millipore) after fixation of cryosections with acetone. As secondary antibody, Alexa 488 anti-rabbit antibody (Invitrogen) was used.

Subcutaneous tumor model

Flank injection of human glioma cells and systemic depletion of NK cells were conducted as described previously (34). Briefly, 1×10^7 human LN-229 *B7H3* knockdown cells or LN-229 sh-Ctrl. cells were injected subcutaneously into the right flank of *CD1 nu/nu* mice after mixing with an equal volume of liquid Matrigel (BD Matrigel Basement Membrane Mix; BD Biosciences). NK cell depletion was conducted by biweekly intraperitoneal injection of 1.5 μg/mL of rabbit anti-asialo GM1 antibody (Wako Chemicals) starting 2 days before tumor cell injection. Controls were injected with rabbit IgG (Calbiochem). Tumor growth was regularly monitored using metric calipers accordingly. Flow cytometric analysis of spleen cells with rat anti-mouse Dx5 (Ly49B) antibody from Caltag confirmed NK cell depletion. After 20 days, the mice were sacrificed, tumors were excised, and weighed.

Immunohistochemistry

Formalin-fixed, paraffin-embedded tissue of human diffuse astrocytomas (WHO grade II, $n = 3$), anaplastic astrocytomas (WHO grade III, $n = 7$), and glioblastoma (WHO grade IV, $n = 13$) were provided by the Department of Neuropathology, Institute of Pathology, University Hospital Heidelberg, Heidelberg, Germany. Sections cut to 3 μm were processed using a Ventana BenchMark XT immunostainer (Ventana Medical Systems). Staining procedure included a pretreatment with cell conditioner 1 (pH 8) for 60 minutes, followed by incubation with either goat anti-human B7H3 antibody (1:200; R&D) or mouse anti-human CD8 (1:50; Dako) at 37°C for 32 minutes and for detection of B7H3, application of rabbit anti-goat immunoglobulins (P0446; DAKO) for 32 minutes at room temperature. Incubation was followed by Ventana standard signal amplification, UltraWash, counterstaining with one drop of hematoxylin for 4 minutes and one drop of bluing reagent for 4 minutes. For visualization, ultraView Universal DAB Detection Kit (Ventana Medical Systems) was used. For quantitative analysis of the B7H3 staining pattern, the immunoreactive score (IRS) was applied. IRS was calculated as product of staining intensity and percentage of positive cells, determined as follows: staining intensity was subdivided into 4 groups: 0 (negative), 1 (weak), 2 (moderate),

and 3 (strong). Percentage of positive cells was regarded as 0 (none), 1 (<10%), 2 (10%–50%), 3 (51%–80%), and 4 (>80% positive tumor cells). Infiltration of CD8-positive cells was assessed in 4 glioblastoma with high (IRS > 8) and 4 glioblastoma with low (IRS < 8) B7H3 immunoreactivity. Of each case, four 200× magnification fields were analyzed. Presence of respective cells was scored as 0 (no positive cells), 1 (single positive cells), 2 (single groups of positive cells), or 3 (several groups of >3 positive cells).

Fluorescent immunohistochemistry

The B7H3 colocalization studies on cryosections of human glioblastoma tissue samples were conducted after acetone fixation and staining with a goat polyclonal anti-human B7H3 antibody (R&D), a mouse anti-human CD31 antibody (Dako), a mouse anti-human α-smooth muscle actin (SMA) antibody (Sigma-Aldrich), and a rabbit anti-human nestin (Millipore). As secondary antibodies, a donkey anti-mouse Cy3 antibody (Dianova) and an Alexa 750 goat anti-rabbit antibody (Invitrogen) were used. Finally, sections were counterstained with 4′,6-diamidino-2-phenylindol (DAPI) and analyzed with a Zeiss Axio Observer Z1 immunofluorescence microscope (Zeiss).

Clinical survival data

Queries of the Repository of Molecular Brain Neoplasia Data (REMBRANDT, National Cancer Institute, Bethesda, MD) for CD276 were conducted online in 2011 following the webpage's instructions.

Statistical analysis

Statistical significance was assessed by the Student *t* test (Excel, Microsoft). All *in vitro* experiments reported here were carried out at least 3 times in triplicate or more. For *in vivo* experiments, 5 animals per group were operated. Survival data were plotted by the Kaplan–Meier method and analyzed by the log-rank test.

Results

B7H3 is expressed in human glioma tissue specimens and cultured glioma cells

B7H3 is detected in specimens of freshly dissected human glioma tissue by immunohistochemistry and is markedly upregulated in glioma tissue compared with the surrounding brain tissue at the infiltration zone (Fig. 1A). Here, strong B7H3 expression is found in close proximity to blood vessels. The degree of B7H3 expression correlated with the grade of malignancy of different gliomas (Fig. 1A). All of 18 glioblastoma samples, tested by immunohistochemistry (13 samples) and immunofluorescence analysis (5 samples), were positive for B7H3 (Figs. 1A and C and 4D). Queries of the NIH's REMBRANDT brain tumor database, based on Affymetrix gene expression data and survival data, indicated in addition a correlation between decreased survival and increased gene expression of B7H3 in anaplastic astrocytomas (WHO grade III). In glioblastoma, this correlation is just under the level of significance (Fig. 1B).

To further characterize the localization of the focally enhanced B7H3 expression, costainings with CD31 for endothelial cells, SMA for pericytes, or nestin for glioma cells were conducted (Fig. 1C). These colocalization studies revealed that B7H3 is expressed by endothelial cells and also weakly by SMA-positive cells but in particular by the primary glioma cells surrounding the vessels [Fig. 1C (I)]. On the cellular level, B7H3 protein was expressed in the cytoplasm and on cell membranes.

Moreover, 4 GIC cultures (Supplementary Fig. S1), which were established from human glioblastoma tissue and kept under stem cell conditions, expressed B7H3 mRNA, as did 5 of 5 glioma cell lines. To rule out that expression of 4IgB7H3 in vessels of brain tumor tissue (Fig. 1) is due to soluble B7H3 from the glioma cells themselves, we conducted expression studies of B7H3 in cultivated human pericytes and HCMECs. The expression detected in HCMECs and pericytes was weaker than in tumor cells (Fig. 2A). B7H3 protein of the predicted size of approximately 100 kDa was detectable in all tested glioma cultures (Fig. 2A, top), but the 45-kDa 2IgB7H3 could not be detected in the glioma samples. Finally, B7H3 was detected on the surface of glioma cell lines and GIC cultures as assessed by flow cytometry (Fig. 2A). There was no significant difference in B7H3 expression between GIC cultures and cell lines (Fig. 2A).

In an attempt to detect the recently published (22) soluble 16.5-kDa fragment of B7H3 in cell culture supernatants, we used 2 different antibodies: one directed against a peptide sequence in the first N-terminal immunoglobulin-like extracellular domain and the other one detecting the entire extracellular protein moiety of 2IgB7H3 and in addition due to sequence homology also 4IgB7H3 (Supplementary Fig. S3). The existence of a 16.5-kDa fragment could be substantiated neither in supernatant of glioma cell line cultures nor GIC cultures with these commercial antibodies (Fig. 2B).

To further analyze the mechanism of soluble 4IgB7H3 secretion, we first examined whether 4IgB7H3 could be detected in the exosomal compartment of LN-229 cells. Indeed, 4IgB7H3 colocalized with the exosomal marker CD9 (34) after exosome preparation but was not detected in the unconcentrated supernatant fraction (Fig. 2C). Comparing 4IgB7H3 originating from cell lysates directly with its secreted form obtained from cell culture supernatants, a size difference of about 5 to 7 kDa was detected in immunoblot analyses (Fig. 2D). In nanoLC ESI-MS/MS analyses, this size difference was confirmed, due to a missing peptide sequence of about 7 kDa in the supernatant probe. This part represents the intracellular and transmembrane fragment of 4IgB7H3 (Fig. 2D), which is not present in the concentrated supernatant fraction analyzed by two different antibodies. From this, we assume that after exosomal release of 4IgB7H3 by glioma cells, a 93-kDa fragment is processed and can be detected in concentrated supernatant. 4IgB7H3 appears to be the major isoform of B7H3 expressed in glioblastoma.

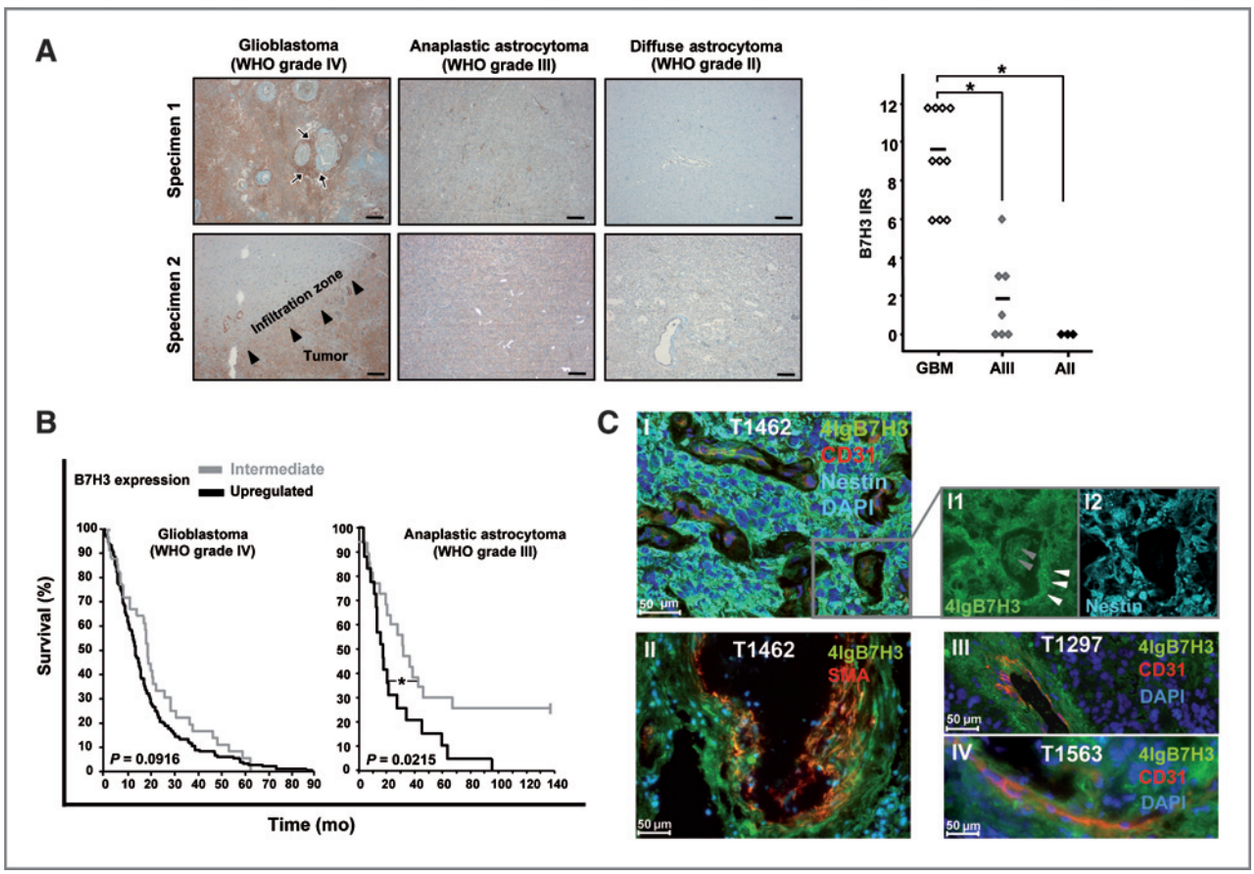

Figure 1. Expression of B7H3 in human glioma tissue and correlation with the grade of malignancy. A, gliomas of different WHO grade were analyzed for B7H3 expression by immunohistochemistry. Representative figures and statistical analysis are presented. B7H3 expression is enhanced in proximity to the blood vessels (specimen 1, arrows). Specimen 2 shows upregulated B7H3 in the tumor compared with the surrounding brain tissue (arrowheads). *, $P < 0.05$ for grade II or III astrocytoma versus GBM. B, Kaplan–Meier survival plot according to Rembrandt queries shows survival rates of glioma patients with intermediate and high B7H3 expression levels. C, immunofluorescence microscopy (I–IV) was applied to detect B7H3 in 3 different glioblastoma specimens (T1462, T1297, T1563). Vessels are visualized by CD31 staining, pericytes are stained with α-SMA, glioma cells are marked by nestin staining, nuclei are counterstained with DAPI. I1 and I2, glioblastoma cells (white arrowheads) surrounding blood (gray arrowheads) vessels exhibit a higher expression of B7H3.

4IgB7H3 is released into the supernatant and inhibits NK-mediated lysis of glioma cells *in vitro* and *in vivo*

We next evaluated the functional activity of 4IgB7H3 expressed by glioma cells. 4IgB7H3 was silenced in the glioma cell line LN-229 with a lentiviral system. The initial knockdown has been about 80% effective; after clonal selection, the knockdown reached 93% in clone 19 on the mRNA level. Immunoblot and flow cytometry reveal a clear reduction of 4IgB7H3 protein levels in lysates, supernatant, and on the surface of the knockdown cells (Fig. 3A). Of note, the transfectants and control cells do not differ in morphology, generation time, or clonogenicity (data not shown). LN-229 sh-4IgB7H3 cells were more susceptible to NK cell–mediated lysis. The clonal knockdown was lysed best with around 60% specific lysis at a target-to-effector cell ratio of 1:30, the less efficient B7H3-silenced pool transfectants showed an intermediate lysis at 40% whereas the controls were at 25% (Fig. 3B, left). Given that 4IgB7H3 is released into the supernatant, we also analyzed whether soluble glioma cell–derived 4IgB7H3 suppresses NK cell–mediated lysis. Hence, we conducted NK lysis assays with LN-229 sh-4IgB7H3 clone 19 cells, which were susceptible to lysis, and supplemented supernatant of LN-229 sh-4IgB7H3 clone 19 or control cells. Compared with the specific NK-mediated lysis of LN-229 sh-4IgB7H3 clone 19 cells of around 60%, the specific lysis of these cells was reduced to 20% by coincubation with concentrated supernatant of control cells. This reduction of specific lysis was weaker after diluting the control supernatant 1:100. The supernatant of LN-229 sh-4IgB7H3 clone 19 cells does not reduce the lysis of LN-229 sh-4IgB7H3 clone 19 cells (Fig. 3B, right). We also generated 4IgB7H3-knockdown cells of the GIC culture T269, with a knockdown of 80% on mRNA level and a significant reduction on protein level measured by immunoblot and flow cytometry (Fig. 3C). T269 sh-4IgB7H3 cells, too, have been significantly more susceptible to NK cell–mediated lysis (Fig. 3D). Taken together, these data indicate that 4IgB7H3 and its secreted form suppress NK cell–mediated lysis of glioma cells and GICs *in vitro*.

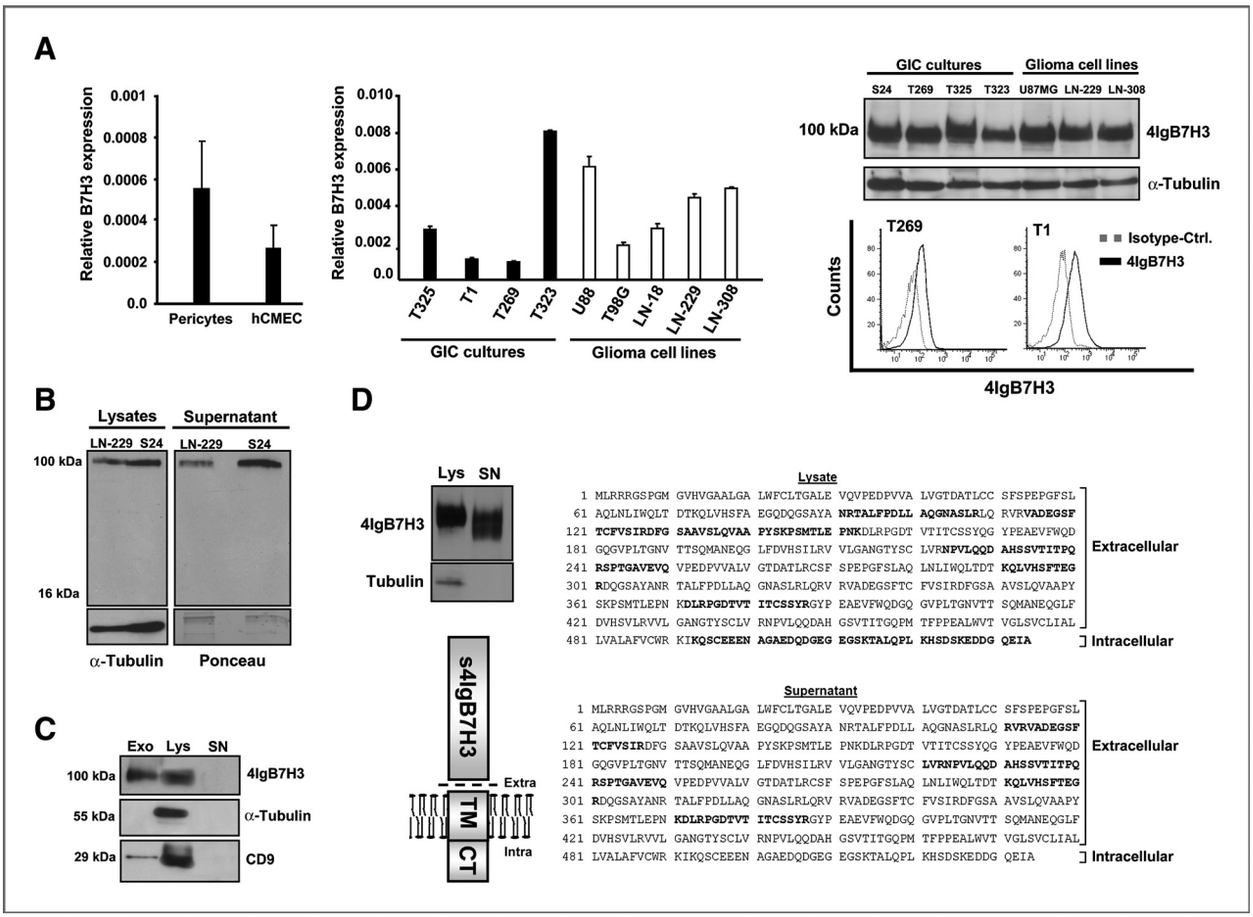

Figure 2. Expression and secretion of 4IgB7H3 by glioma cells, pericytes, and endothelial cells. A, expression of 4IgB7H3 in pericytes and endothelial cells as well as GIC (black bars) and glioma cell lines (white bars) on mRNA or protein levels (right top) and on the cell surface of GIC cultures (right bottom) is presented. B, 4IgB7H3 in LN-229 glioma cells and GIC culture S24 was detected in lysates and in concentrated supernatant. A 93-kDa fragment was substantiated in the supernatant but no 16.5-kDa fragment. α-Tubulin was chosen as loading control for cell lysates and Ponceau staining for supernatant. C, exosome (Exo) preparation shows that 4IgB7H3 is released within the exosomal compartment from the glioma cell line LN-229. CD9 staining was used as an exosomal marker. Unconcentrated supernatants (SN) are negative whereas lysates (Lys) are positive for 4IgB7H3 and CD9. D, protein size analyses of 4IgB7H3 in LN-229 whole-cell lysates and concentrated supernatant by immunoblot show size differences of whole and soluble 4IgB7H3 (s4IgB7H3). Positions of identified peptides (bold letters) in human 4IgB7H3 amino acid sequence derived from lysates and supernatant analyzed by nanoLC-ESI-MS/MS (right) as well as illustrative sketch visualizing hypothetical position of soluble 4IgB7H3 processing (interrupted line). CT, cytoplasmic tail; TM, transmembrane.

To further characterize the impact of 4IgB7H3 expression *in vivo*, subcutaneous tumors were generated with LN-229 sh-4IgB7H3 and control cells. Tumor growth was monitored in LN-229 sh-4IgB7H3 and control cells in NK cell–depleted compared with control IgG antibody–treated mice (35). Here, a significant difference in tumor growth and tumor weight at the end of the experiment was only detected between LN-229 sh-4IgB7H3–derived tumors in NK cell–depleted versus nondepleted animals. In NK cell–retaining animals, LN-229 sh-4IgB7H3–derived tumors grew significantly smaller and were lighter at the end of the experiment. In LN-229 sh-control–derived tumors, NK cell depletion had no significant impact on tumor growth and weight (Fig. 4A and B) showing that silencing of 4IgB7H3 made glioma cells susceptible to NK cell–dependent cytotoxicity. Moreover, human glioblastoma samples showed a highly significant inverse correlation between B7H3 expression and invasion of CD8-positive immune cells. Costaining of B7H3 and CD8 revealed that the influx of CD8-positive cells is significantly higher in B7H3-low–expressing tumors than in B7H3-high–expressing tumors (Fig. 4C and D)

Regulation and cleavage of 4IgB7H3 in glioma cells differ from other tumor entities and immune cells

To evaluate how 4IgB7H3 expression is regulated and how soluble 4IgB7H3 is cleaved from the cell surface, we assessed the influence of protein kinase C activation PMA, inhibition of MMP by ilomastat (22), inhibition of TGF-β with LY2157299 or a furin inhibitor, and hypoxia on 4IgB7H3 levels. All compounds are sufficiently active in control assays (data not shown). 4IgB7H3 was neither induced by PMA on mRNA level nor on the protein level in cell lysates or with regard to the 93-kDa soluble form in the supernatant of glioma cells (Supplementary Fig. S2A).

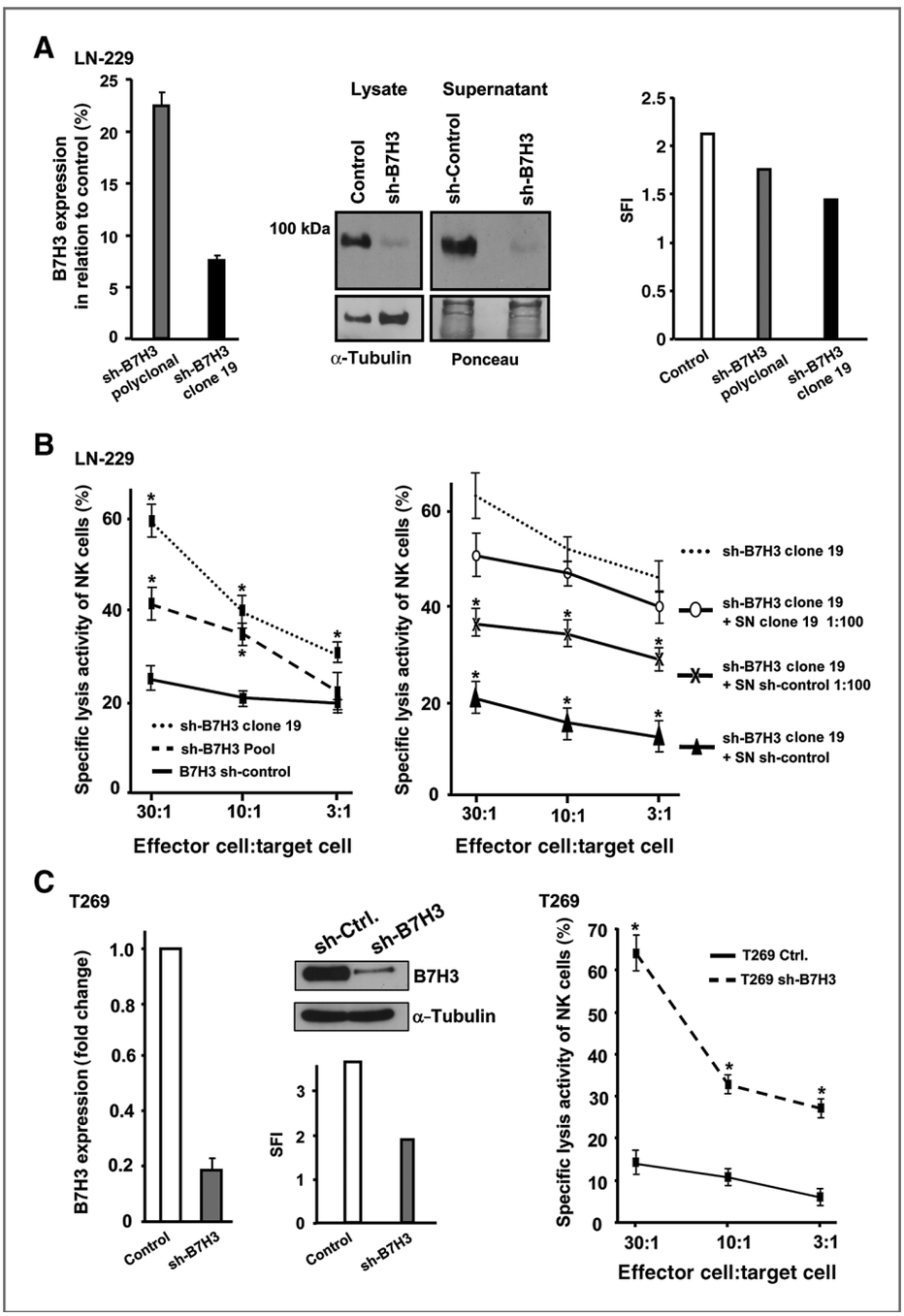

Figure 3. Increased susceptibility of LN-229 4IgB7H3 sh-cells to NK cell–mediated lysis. A, polyclonal knockdown and clonal selection (clone 19) of 4IgB7H3 in LN-229 cells were conducted. Knockdown efficiency on mRNA level (left), protein level (middle), and on the cell surface evaluated by flow cytometry are illustrated (right). B, LN-229 sh-4IgB7H3 (polyclonal or clone 19), sh-control cells, or LN-229 sh-4IgB7H3 (left) as well as clone 19 cells supplemented with supernatant (SN) derived from clone 19 or control cells (right) were incubated with activated NK cells for 4 hours at the indicated effector-to-target cell ratios. C, knockdown of 4IgB7H3 in GIC culture T269 was conducted and efficiency evaluated on mRNA level by qPCR (left), on protein level by immunoblot analysis and by flow cytometry (right). D, activated NK cells were incubated with T269 sh-4IgB7H3 or sh-control cells and NK cell–mediated lysis (%) has been evaluated. Representative results from three independent NK lysis experiments are depicted. Data represent mean and SEM; $n = 5$; *, $P < 0.05$ relative to controls.

Moreover, cleavage of 4IgB7H3 from the surface of the glioma cell line LN-229 (Supplementary Fig. S2B) and GIC cultures T325 (Supplementary Fig. S2A and S2B) was not influenced by inhibition of MMPs with ilomastat as shown before for monocytes, dendritic cells, activated T cells, and various carcinoma cells. Inhibition of TGF-β, which is known to suppress NK cells and to convey immune escape of gliomas in various manners (36), did not result in downregulation of 4IgB7H3, nor did hypoxia influence its expression (Supplementary Fig. S2A). Further experiments evaluating the regulation of 4IgB7H3 in glioma cells did not show a significant upregulation of 4IgB7H3 on the mRNA level, nor in the supernatant of LN-229 cells following irradiation, IFN-γ, dexamethasone, or H_2O_2 treatment (Supplementary Fig. S2C).

4IgB7H3 modulates the invasive phenotype in glioma cells *in vitro* and *in vivo*

Mounting evidence suggests that 4IgB7H3 is involved in tumor cell migration and invasiveness. Therefore,

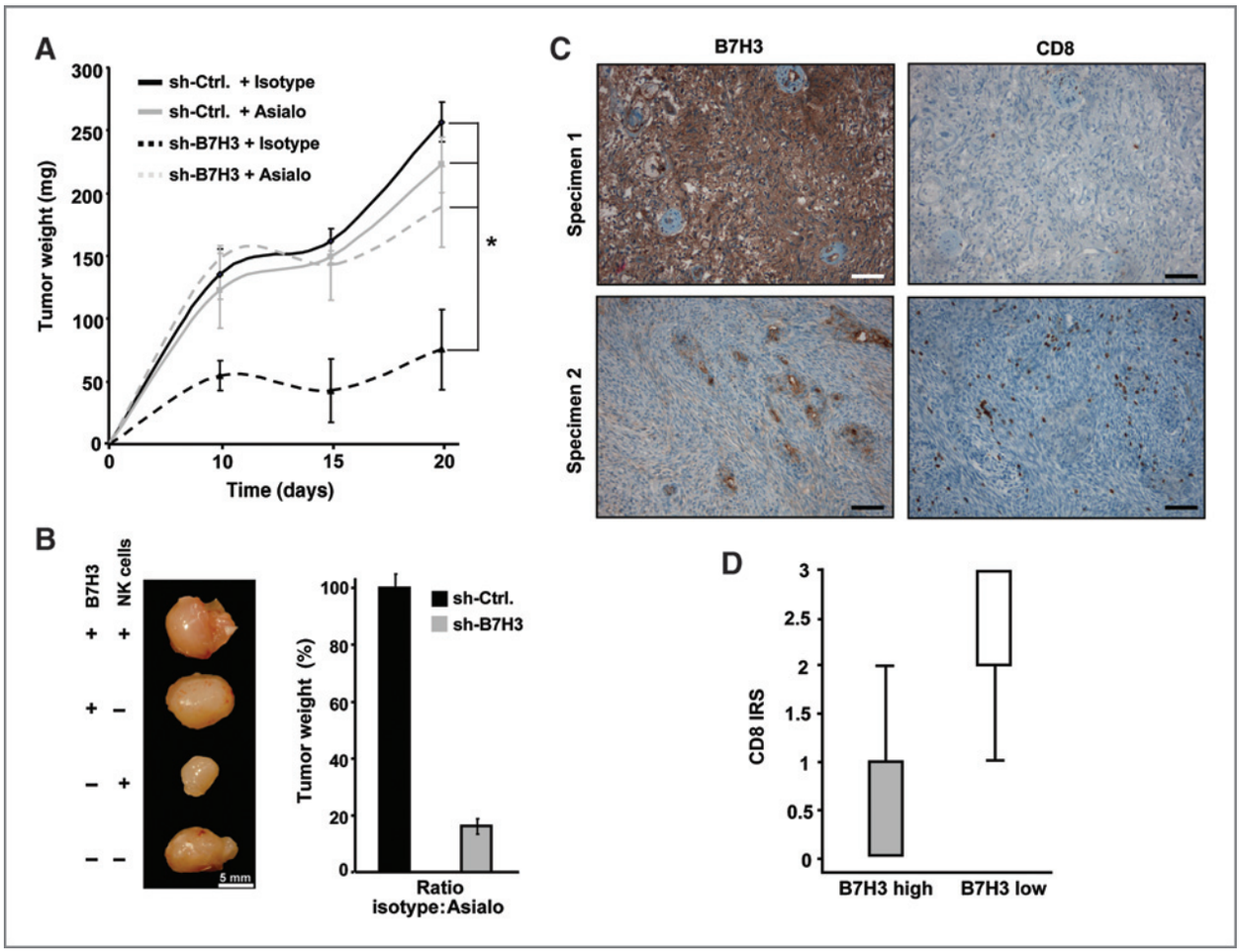

Figure 4. B7H3 exerts an immunosuppressive function *in vivo*. A, tumor size of subcutaneously injected LN-229 shB7H3 and control cells were monitored in NK cell–depleted (+Asialo) and control-treated (+Isotype) animals. Only the tumors which developed from LN-229 shB7H3 cells growing in mice with NK cells (dotted line) are significantly smaller. *, $P < 0.05$ for tumors of control-treated animals versus Asialo treatment or sh-B7H3. B, representative images of explanted tumors and statistical analysis of tumor weight at the end of the experiment. C, B7H3-high–expressing human glioblastoma tissue (specimen 1) shows a reduced infiltration of CD8-positive immune cells compared with B7H3-low–expressing human glioblastoma tissue (specimen 2). D, statistical analysis of B7H3-high- and -low–expressing human glioblastoma tissues shows a stronger invasion of CD8-positive cells in B7H3-low–expressing tumors.

Boyden chamber Matrigel and spheroid invasion assays were conducted with LN-229 cells as well as with the GIC culture T269. LN-229 sh-4IgB7H3 cells displayed reduced transmigration compared with control cells in these assays (Fig. 5A). Interestingly, the invasive phenotype was partly restored in LN-229 sh-4IgB7H3 cells when invasion assays were conducted with supplementation of concentrated supernatant of LN-229 control cells (Fig. 5B). There was also a reduction in the invasiveness of LN-229 control cells when the cells were incubated with supernatant from LN-229 sh-4IgB7H3 cells instead of supernatant from control cells during the invasion experiments (Fig. 5B), indicating that glioma supernatant may have an anti-invasive property, which can be partly overcome by the proinvasive effect of soluble 4IgB7H3. To verify this proinvasive effect of 4IgB7H3 in primary glioma cells, primary 4IgB7H3–silenced T269 GICs were further used in a functional invasion assay. This spheroid invasion assay showed a significant reduction of the invasive phenotype in T269 cells after 4IgB7H3 gene silencing (Fig. 5C).

Aiming at confirming the *in vitro* data in an *in vivo* model, T269 sh-4IgB7H3 knockdown or control cells were orthotopically implanted into the brains of CD1 *nu*/*nu* mice. Ten weeks later, animals were sacrificed and tumor invasion was assessed by staining of the tumor cells with anti-human nestin antibody. Brain sections displayed a highly infiltrative tumor growth pattern with tumor cells reaching brain regions in the ipsilateral and contralateral hemisphere far off the implantation site in T269 control xenograft animals (Fig. 6, top). In contrast, clearly defined bulky tumors were found in T269 sh-4IgB7H3–xenografted brains without detectable tumor cells in ipsilateral or contralateral brain regions distant from the implantation site (Fig. 6, bottom).

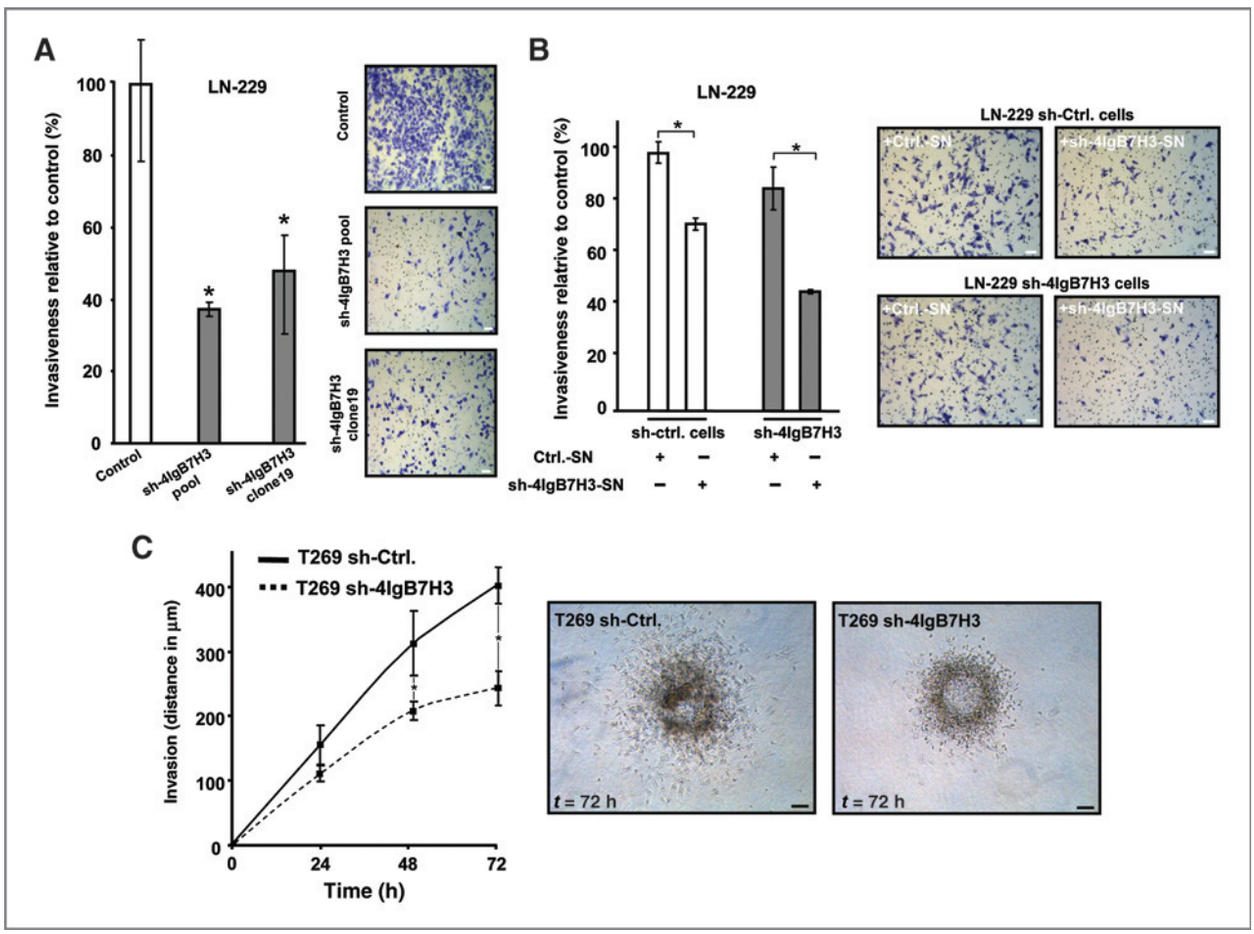

Figure 5. 4IgB7H3 mediates a proinvasive phenotype in glioma cells *in vitro*. A, LN-229 sh-4IgB7H3 (polyclonal knockdown and clone 19) and sh-control glioma cells or (B) clone 19 and sh-control cells incubated each with concentrated supernatant (SN) of control or clone 19 cells were analyzed for invasiveness in a Matrigel invasion chamber assay. Invaded cells were counted in 5 independent fields. Invasion is expressed as percentage in relation to sh-control cells without supernatant (scale bars: 100 µm; data represent mean and SEM; $n = 3$; *, $P < 0.05$). Representative images of the Boyden chambers are depicted. C, T269 control or sh-4IgB7H3 cells were analyzed for their invasive properties in a spheroid invasion assay. The area covered by invaded cells from each spheroid was measured in intervals of 24 hours. Data represent mean and SEM ($n = 3$). Representative glioma spheroids are shown (scale bars: 100 µm).

Discussion

Glioblastoma is a paradigmatic tumor for tumor-associated immunosuppression. B7H3 is a novel member of the B7-family of costimulatory proteins. As parts of our efforts to characterize and understand the immune phenotype of glioblastoma, we here report that B7H3 is expressed in human glioblastoma tissue by both glioblastoma and endothelial cells (Figs. 1 and 2A). Glioma cells that surround the blood vessels preferentially express B7H3. In addition to that, expression correlates significantly with increasing tumor grade and is associated with poor survival within WHO grade III gliomas.

By mass spectrometry and immunoblot analysis, we identified that 4IgB7H3 but not the smaller isoform 2IgB7H3 was preferentially expressed by different GIC cultures and glioma cell lines what was not determined in immunohistochemical analysis because of the lack of isoform-specific antibodies (Supplementary Fig. S3). Furthermore, it was showed that 4IgB7H3 is secreted in exosomes into the supernatant of glioma cells and finally processed to a soluble form of about 93 kDa. Interestingly, this soluble 4IgB7H3 is not the 16.5-kDa soluble form of B7H3 postulated in nonmalignant and malignant cells before (22). Although two different antibodies were used, the one detecting whole extracellular protein and the other one being the first immunoglobulin-like domain of the extracellular N-Terminus, we could not detect the published fragment of about 16.5 kDa in the supernatant of glioma cells. Here, the soluble fragment was about 7 kDa smaller than 4IgB7H3 originating from cell lysates (Fig. 2). In an attempt to further characterize

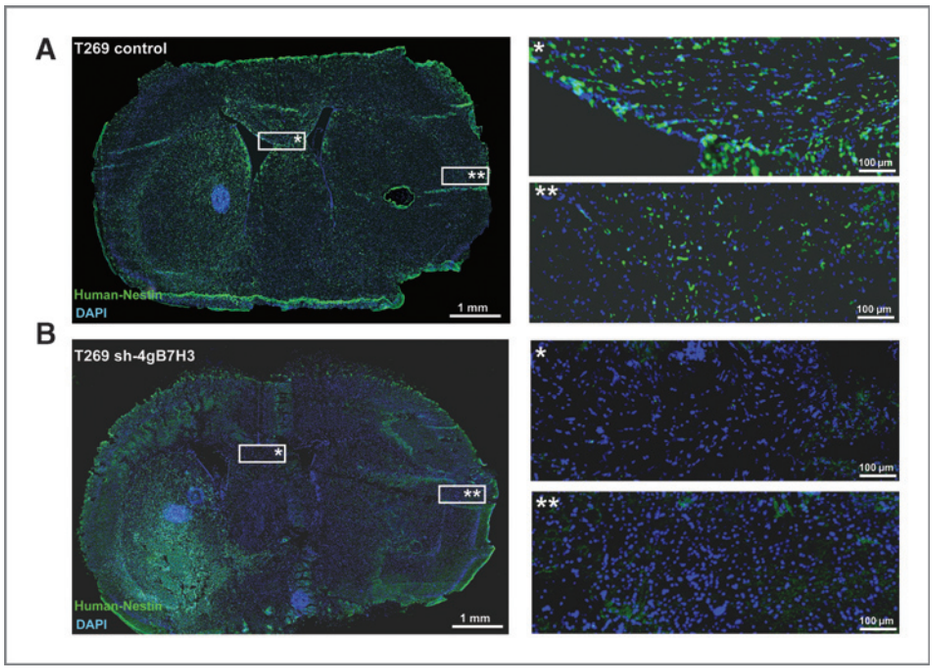

Figure 6. 4IgB7H3 drives the proinvasive phenotype of glioblastoma *in vivo*. Immunohistologic analysis of (A) T269 control and (B) T269 sh-4IgB7H3 tumor–bearing CD1 *nu/nu* mice. T269 tumor cells were detected by immunofluorescent anti-human nestin staining. Asterisks show areas with a higher magnification.

the regulation and cleavage mechanism of B7H3 in glioblastoma, the cells were incubated with PMA, which was published to induce B7H3 on immune and tumor cells (9, 37). This regimen had no effect on B7H3 expression in glioblastoma cells on mRNA or protein level, neither did the inhibition of MMP, which have been suggested to cleave soluble B7H3 from the surface of tumor cells (22). We finally evaluated whether blockage of TGF-β activation with a furin inhibitor in the glioblastoma cell line LN-229 influenced 4IgB7H3 expression because TGF-β is known to be responsible for a variety of immunosuppressive and proinvasive effects (5, 6, 8, 20). However, TGF-β inhibition did neither result in the downregulation of 4IgB7H3 nor its soluble form (Supplementary Fig. S2).

Importantly, 4IgB7H3 was functional in the glioblastoma cell line LN-229 and the GIC culture T269 and suppressed NK cell–mediated tumor lysis *in vitro* (Fig. 2) as well as *in vivo (*Fig. 3*)*. In attempt to elucidate the immunosuppressive function of B7H3 in human glioblastoma, we conducted colocalization studies of B7H3 expression and CD8-positive cells. Here, a significant higher influx of CD8-positive cells in B7H3-low–expressing tumors was detected than B7H3-high–expressing tumors. As CD8 is a marker for cytotoxic T cells which were also published to be suppressed by B7H3 (20) and NK cells, these data provide further evidence for an immunosuppressive function of B7H3. Furthermore, 4IgB7H3 exerted a proinvasive effect in glioblastoma cells *in vitro* (Fig. 5). We could additionally show the proinvasive effect of 4IgB7H3 in the GIC compartment *in vivo*: The highly invasive phenotype of the GIC culture T269 was significantly reduced by *4IgB7H3* gene silencing (Fig. 6). Interestingly, native glioblastoma-derived soluble 4IgB7H3 suppresses NK lysis and enhances glioblastoma cell invasiveness *in vitro*. Insofar, our data let us to postulate that NK cell suppression and the proinvasive effect attributed to 4IgB7H3 expression in different tumor entities (37) are in fact exerted by membrane-bound and soluble B7H3, which was until now only evaluated for its diagnostic and prognostic capacity (22, 23, 38). Finally, as soluble 4IgB7H3 was sufficient to restore the invasiveness of 4IgB7H3-silenced LN-229 cells, the presence of a yet unknown counter-receptor must be postulated on glioblastoma cells, too.

To summarize, our data provide new insights on the role of B7H3 expression in glioblastoma. There is an immunosuppressive function of 4IgB7H3 in glioblastoma similar to other tumor entities. This is also true for a proinvasive phenotype. These effects can be exerted by secreted soluble 4IgB7H3 on its own leading to the assumption that the yet unidentified counter-receptor is expressed on immune and glioblastoma cells. Glioblastoma unlike nonmalignant cells do not generate and release the 16.5-kDa B7H3 fragment into the supernatant analyzed by commercially available antibodies. Our data support a fragment of about 93 kDa to exert that effect rather than a small 16.5-kDa fragment.

These data provide a therapeutic rationale to ameliorate treatment of glioblastoma by blockage of 4IgB7H3. First attempts to use 4IgB7H3 as a therapeutic target have been made recently with an antibody against 4IgB7H3 used to track neuroblastoma cells without intending to block 4IgB7H3 function itself (39) and a pseudomonas immunotoxin-coupled anti-B7H3 antibody to track glioblastoma xenograft tumors (40). Further experiments are needed to

evaluate 4IgB7H3 as a target in the treatment of 4IgB7H3-expressing tumors.

Disclosure of Potential Conflicts of Interest

No potential conflicts of interest were disclosed.

Acknowledgments

The authors thank Marius Lemberg (Center for Molecular Biology, University of Heidelberg, Heidelberg, Germany) for advice with the exosome preparation and are grateful for the support by the Microscopy Core Facility and the Department of Molecular Genetics (B. Radlwimmer) of the German Cancer Research Center Heidelberg, Heidelberg, Germany.

Grant Support

This work was supported within the Brain Tumor Network BTNplus (Subproject 14; FKZ 01GS0883) of the National Genome Research Network (NGFNplus) by the Federal Ministry of Education and Research (BMBF), and the Charitable Hertie Foundation.

The costs of publication of this article were defrayed in part by the 649 payment of page charges. This article must therefore be hereby marked 650 advertisement in accordance with 18 U.S.C. Section 1734 solely to indicate 651 this fact.

Received April 4, 2011; revised October 28, 2011; accepted October 31, 2011; published OnlineFirst November 11, 2011.

References

1. Dietrich PY. Antitumor immune response: what are the roles for gliomas?. Rev Neurol (Paris) 2001;157:1339–48.
2. Eisele G, Wischhusen J, Mittelbronn M, Meyermann R, Waldhauer I, Steinle A, et al. TGF-beta and metalloproteinases differentially suppress NKG2D ligand surface expression on malignant glioma cells. Brain 2006;129:2416–25.
3. Friese MA, Wischhusen J, Wick W, Weiler M, Eisele G, Steinle A, et al. RNA interference targeting transforming growth factor-beta enhances NKG2D-mediated antiglioma immune response, inhibits glioma cell migration and invasiveness, and abrogates tumorigenicity *in vivo*. Cancer Res 2004;64:7596–603.
4. Heimberger AB, Kong LY, Abou-Ghazal M, Reina-Ortiz C, Yang DS, Wei J, et al. The role of tregs in human glioma patients and their inhibition with a novel STAT-3 inhibitor. Clin Neurosurg 2009;56:98–106.
5. Roth P, Aulwurm S, Gekel I, Beier D, Sperry RG, Mittelbronn M, et al. Regeneration and tolerance factor: a novel mediator of glioblastoma-associated immunosuppression. Cancer Res 2006;66:3852–8.
6. Roth P, Mittelbronn M, Wick W, Meyermann R, Tatagiba M, Weller M. Malignant glioma cells counteract antitumor immune responses through expression of lectin-like transcript-1. Cancer Res 2007;67:3540–4.
7. Sampson JH, Archer GE, Mitchell DA, Heimberger AB, Bigner DD. Tumor-specific immunotherapy targeting the EGFRvIII mutation in patients with malignant glioma. Semin Immunol 2008;20:267–75.
8. Weller M, Fontana A. The failure of current immunotherapy for malignant glioma. Tumor-derived TGF-beta, T-cell apoptosis, and the immune privilege of the brain. Brain Res Brain Res Rev 1995;21:128–51.
9. Chapoval AI, Ni J, Lau JS, Wilcox RA, Flies DB, Liu D, et al. B7-H3: a costimulatory molecule for T cell activation and IFN-gamma production. Nat Immunol 2001;2:269–74.
10. Steinberger P, Majdic O, Derdak SV, Pfistershammer K, Kirchberger S, Klauser C, et al. Molecular characterization of human 4Ig-B7-H3, a member of the B7 family with four Ig-like domains. J Immunol 2004;172:2352–9.
11. Zhou YH, Chen YJ, Ma ZY, Xu L, Wang Q, Zhang GB, et al. 4IgB7-H3 is the major isoform expressed on immunocytes as well as malignant cells. Tissue Antigens 2007;70:96–104.
12. Castriconi R, Dondero A, Augugliaro R, Cantoni C, Carnemolla B, Sementa AR, et al. Identification of 4Ig-B7-H3 as a neuroblastoma-associated molecule that exerts a protective role from an NK cell-mediated lysis. Proc Natl Acad Sci U S A 2004;101:12640–5.
13. Crispen PL, Sheinin Y, Roth TJ, Lohse CM, Kuntz SM, Frigola X, et al. Tumor cell and tumor vasculature expression of B7-H3 predict survival in clear cell renal cell carcinoma. Clin Cancer Res 2008;14:5150–7.
14. Roth TJ, Sheinin Y, Lohse CM, Kuntz SM, Frigola X, Inman BA, et al. B7-H3 ligand expression by prostate cancer: a novel marker of prognosis and potential target for therapy. Cancer Res 2007;67:7893–900.
15. Sun Y, Wang Y, Zhao J, Gu M, Giscombe R, Lefvert AK, et al. B7-H3 and B7-H4 expression in non-small-cell lung cancer. Lung Cancer 2006;53:143–51.
16. Yamato I, Sho M, Nomi T, Akahori T, Shimada K, Hotta K, et al. Clinical importance of B7-H3 expression in human pancreatic cancer. Br J Cancer 2009;101:1709–16.
17. Zang X, Thompson RH, Al-Ahmadie HA, Serio AM, Reuter VE, Eastham JA, et al. B7-H3 and B7x are highly expressed in human prostate cancer and associated with disease spread and poor outcome. Proc Natl Acad Sci U S A 2007;104:19458–63.
18. Seaman S, Stevens J, Yang MY, Logsdon D, Graff-Cherry C, St CB. Genes that distinguish physiological and pathological angiogenesis. Cancer Cell 2007;11:539–54.
19. Hashiguchi M, Kobori H, Ritprajak P, Kamimura Y, Kozono H, Azuma M. Triggering receptor expressed on myeloid cell-like transcript 2 (TLT-2) is a counter-receptor for B7-H3 and enhances T cell responses. Proc Natl Acad Sci U S A 2008;105:10495–500.
20. Leitner J, Klauser C, Pickl WF, Stöckl J, Majdic O, Bardet AF, et al. B7-H3 is a potent inhibitor of human T-cell activation: no evidence for B7-H3 and TREML2 interaction. Eur J Immunol 2009;39:1754–64.
21. Sun J, Chen LJ, Zhang GB, Jiang JT, Zhu M, Tan Y, et al. Clinical significance and regulation of the costimulatory molecule B7-H3 in human colorectal carcinoma. Cancer Immunol Immunother 2010;59:1163–71.
22. Zhang G, Hou J, Shi J, Yu G, Lu B, Zhang X. Soluble CD276 (B7-H3) is released from monocytes, dendritic cells and activated T cells and is detectable in normal human serum. Immunology 2008;123:538–46.
23. Zhang G, Xu Y, Lu X, Huang H, Zhou Y, Lu B, et al. Diagnosis value of serum B7-H3 expression in non-small cell lung cancer. Lung Cancer 2009;66:245–9.
24. Hermisson M, Klumpp A, Wick W, Wischhusen J, Nagel G, Roos W, et al. O6-methylguanine DNA methyltransferase and p53 status predict temozolomide sensitivity in human malignant glioma cells. J Neurochem 2006;96:766–76.
25. Svendsen CN, ter Borg MG, Armstrong RJ, Rosser AE, Chandran S, Ostenfeld T, et al. A new method for the rapid and long term growth of human neural precursor cells. J Neurosci Methods 1998;85:141–52.
26. Rieger J, Lemke D, Maurer G, Weiler M, Frank B, Tabatabai G, et al. Enzastaurin-induced apoptosis in glioma cells is caspase-dependent and inhibited by BCL-XL. J Neurochem 2008;106:2436–48.
27. Burghardt I, Tritschler F, Opitz CA, Frank B, Weller M, Wick W. Pirfenidone inhibits TGF-beta expression in malignant glioma cells. Biochem Biophys Res Commun 2007;354:542–7.
28. Weiler M, Bähr O, Hohlweg U, Naumann U, Rieger J, Huang H, et al. BCL-xL: time-dependent dissociation between modulation of apoptosis and invasiveness in human malignant glioma cells. Cell Death Differ 2006;13:1156–69.
29. Jang BC, Park YK, Choi IH, Kim SP, Hwang JB, Baek WK, et al. 12-O-tetradecanoyl phorbol 13-acetate induces the expression of B7-DC, -H1, -H2, and -H3 in K562 cells. Int J Oncol 2007;31:1439–47.

30. Leitlein J, Aulwurm S, Waltereit R, Naumann U, Wagenknecht B, Garten W, et al. Processing of immunosuppressive pro-TGF-beta 1,2 by human glioblastoma cells involves cytoplasmic and secreted furin-like proteases. J Immunol 2001;166:7238–43.
31. Opitz CA, Litzenburger UM, Lutz C, Lanz TV, Tritschler I, Köppel A, et al. Toll-like receptor engagement enhances the immunosuppressive properties of human bone marrow-derived mesenchymal stem cells by inducing indoleamine-2,3-dioxygenase-1 via interferon-beta and protein kinase R. Stem Cells 2009;27:909–19.
32. Carraro G, Albertin G, Forneris M, Nussdorfer GG. Similar sequence-free amplification of human glyceraldehyde-3-phosphate dehydrogenase for real time RT-PCR applications. Mol Cell Probes 2005;19:181–6.
33. Wick W, Grimmel C, Wild-Bode C, Platten M, Arpin M, Weller M. Ezrin-dependent promotion of glioma cell clonogenicity, motility, and invasion mediated by BCL-2 and transforming growth factor-beta2. J Neurosci 2001;21:3360–8.
34. Opitz CA, Litzenburger UM, Sahm F, Ott M, Tritschler I, Trump S, et al. An endogenous ligand of the human aryl hydrocarbon receptor promotes tumor formation. Nature 2011;478:197–203.
35. Guescini M, Genedani S, Stocchi V, Agnati LF. Astrocytes and Glioblastoma cells release exosomes carrying mtDNA. J Neural Transm 2010;117:1–4.
36. Wick W, Wild-Bode C, Frank B, Weller M. BCL-2-induced glioma cell invasiveness depends on furin-like proteases. J Neurochem 2004;91:1275–83.
37. Chen YW, Tekle C, Fodstad O. The immunoregulatory protein human B7H3 is a tumor-associated antigen that regulates tumor cell migration and invasion. Curr Cancer Drug Targets 2008;8:404–13.
38. Chen X, Zhang G, Li Y, Feng X, Wan F, Zhang L, et al. Circulating B7-H3 (CD276) elevations in cerebrospinal fluid and plasma of children with bacterial meningitis. J Mol Neurosci 2009;37:86–94.
39. Kramer K, Kushner BH, Modak S, Pandit-Taskar N, Smith-Jones P, Zanzonico P, et al. Compartmental intrathecal radioimmunotherapy: results for treatment for metastatic CNS neuroblastoma. J Neurooncol 2010;97:409–18.
40. Luther N, Cheung NK, Souliopoulos EP, Karampelas I, Bassiri D, Edgar MA, et al. Interstitial infusion of glioma-targeted recombinant immunotoxin 8H9scFv-PE38. Mol Cancer Ther 2010;9:1039–46.